Research Square

Preprints are preliminary reports that have not undergone peer review.
They should not be considered conclusive, used to inform clinical practice,
or referenced by the media as validated information.

Small-Molecule Mimicry Intercepts PEX5 Recognition by Trypanosomal PEX14 as Revealed by Molecular Dynamics

Amanda R. Guimarães

a.ribeiro-guimaraes@kent.ac.uk

University of Kent

Esther R. S. Paz

University of Kent

Allison Serrano-Trejos

Universidad ECCI

Chonny Herrera-Acevedo

Universidad ECCI

Iván Rivilla

Donostia International Physics Center (DIPC)

Oscar R. Ballesteros

Center of Innovation in Advanced Chemistry, Faculty of Chemistry (ORFEO CINQA), University of the Basque Country (UPV/EHU)

Caroline R. Kwawu

Kwame Nkrumah University of Science and Technology

Guilherme A. M. Jardim

Instituto de Ciências Exatas, Universidade Federal de Minas Gerais

Eufrânio N. da Silva Júnior

Instituto de Ciências Exatas, Universidade Federal de Minas Gerais

Felipe Fantuzzi

University of Kent

Research Article

Keywords: PEX5, PEX14, Protein--protein interaction, Protein--ligand interaction, Molecular docking, Molecular dynamics, SuFEx-functionalised naphthoquinones

Posted Date: June 25th, 2026

DOI: https://doi.org/10.21203/rs.3.rs-10027778/v1

License: This work is licensed under a Creative Commons Attribution 4.0 International License.
Read Full License

Additional Declarations: No competing interests reported.

Small-Molecule Mimicry Intercepts PEX5 Recognition by Trypanosomal PEX14 as Revealed by Molecular Dynamics

Amanda R. Guimarães[1*], Esther R. S. Paz[1,2], Allison Serrano-Trejos[3], Chonny Herrera-Acevedo[3], Iván Rivilla[4,5], Oscar R. Ballesteros[5], Caroline R. Kwawu[1,6], Guilherme A. M. Jardim[2], Eufrânio N. da Silva Júnior[2], Felipe Fantuzzi[1]

[1]Supramolecular, Interfacial and Synthetic Chemistry, School of Natural Sciences, University of Kent, Park Wood Rd, Canterbury, CT2 7NH, United Kingdom.
[2]Departamento de Química, Instituto de Ciências Exatas, Universidade Federal de Minas Gerais, Belo Horizonte, 31270–901, MG, Brazil.
[3]Department of Chemical Engineering, Universidad ECCI, Bogotá D.C, 111311, Colombia.
[4]Donostia International Physics Center (DIPC), Manuel Lardizabal Ibilbidea, 4, San Sebastián/Donostia, 20018, Gipuzkoa, Spain.
[5]Department of Organic Chemistry I, Center of Innovation in Advanced Chemistry, Faculty of Chemistry (ORFEO CINQA), University of the Basque Country (UPV/EHU), Av. Tolosa, 72, San Sebastián/Donostia, 20018, Gipuzkoa, Spain.
[6]Department of Chemistry, Kwame Nkrumah University of Science and Technology, Kumasi, UPO, AK-385-1973, Ghana.

*Corresponding author(s). E-mail(s): a.ribeiro-guimaraes@kent.ac.uk;
Contributing authors: e.paz-104@kent.ac.uk; allisonju.serranotr@ecci.edu.co; cherreraa@ecci.edu.co; ivan.rivilla@ehu.eus; oscar.rodriguez@dipc.org; c.kwawu@kent.ac.uk; guilhermeamj@ufmg.br; eufranio@ufmg.br; f.fantuzzi@kent.ac.uk;

Abstract

Human trypanosomiases, including Chagas disease and human African trypanosomiasis, remain major neglected tropical diseases with limited therapeutic options and substantial treatment-associated toxicity. In trypanosomatids, glycolytic enzymes are compartmentalised within glycosomes, peroxisome-like organelles whose biogenesis depends on the essential interaction between the peroxins PEX5 and PEX14. Interference with this protein–protein interface therefore represents a promising strategy for developing new trypanocidal agents. Here, molecular docking, MD simulations, and MM–PBSA calculations were used to examine the PEX5–PEX14 interaction and small-molecule binding to the PEX14 recognition groove. The PEX5–PEX14 complex was stabilised by contacts centred on the canonical Wxxx(F/Y) motif of PEX5, particularly Trp60 and Tyr64, with additional contributions from a secondary non-canonical PEX5 region. Hydrogen bonds, salt bridges, π–cation contacts, and T-shaped aromatic interactions involving PEX14 residues Phe12, Phe29, Lys33, and Thr21 were key contributors to complex stability. The reported inhibitor ET7 reproduced central features of the native PEX5 recognition motif and remained associated with the PEX14 groove throughout the simulations. SuFEx-functionalised naphthoquinones from a previously reported series were then assessed as potential PEX14 ligands. While the initial sulfonyl fluoride derivative associated only transiently with the groove, SuFEx derivatisation at the sulfonyl centre to introduce an additional aromatic substituent increased residence time and gave more favourable MM–PBSA binding free energies. These results identify aromatic and electrostatic contacts as major determinants of ligand stabilisation within the PEX14 groove and support SuFEx-derived naphthoquinones as promising scaffolds for inhibitors targeting glycosomal protein import in *Trypanosoma* species.

Keywords: PEX5–PEX14, Protein–protein interaction, Protein–ligand interaction, Molecular docking, Molecular dynamics, SuFEx-functionalised naphthoquinones

1 Introduction

Human trypanosomiases represent a significant and persistent public health challenge in endemic regions [1–3]. These diseases are caused by protozoan parasites of the genus *Trypanosoma*, notably *T. cruzi*, the aetiological agent of Chagas disease (CD) in the Americas [4], and *T. brucei*, responsible for human African trypanosomiasis (HAT) in sub-Saharan Africa [5]. A distinctive feature of trypanosomatid metabolism is the compartmentalisation of glycolysis, the central pathway by which glucose is converted into smaller metabolites with concomitant energy production. Whereas in most eukaryotic cells glycolysis occurs in the cytosol, in trypanosomatids several glycolytic enzymes are enclosed within glycosomes, specialised peroxisome-like organelles that are essential for parasite viability [6–8]. Because these enzymes are synthesised in the cytosol but function inside glycosomes, they must be imported into the organelle as cargo proteins. Glycosome biogenesis and maintenance therefore depend on a dedicated protein-import machinery formed by peroxins, also known as PEX proteins (Figure 1).

In this import pathway, cargo proteins are directed to glycosomes by short amino-acid sequences known as peroxisomal targeting signals (PTS), which act as molecular address labels. The most common signal, PTS1, is usually located at the *C*-terminal end of cargo proteins and is recognised by the soluble receptor PEX5 through its C-terminal tetratricopeptide repeat (TPR) domain [9–11]. PEX5 therefore acts as a shuttle receptor: it binds folded cargo proteins in the cytosol and delivers them to the glycosomal membrane. This delivery step is mediated by the intrinsically disordered N-terminal region of PEX5, which contains Wxxx(F/Y) motifs. In this notation, W denotes tryptophan, x represents any amino acid, and F/Y indicates either phenylalanine or tyrosine; these short aromatic motifs function as docking elements, particularly for PEX14.

After docking, the cargo is translocated into the glycosomal lumen and the PEX machinery is recycled for additional rounds of import without requiring cargo unfolding [12–14]. This membrane-associated stage involves peroxins such as PEX13 and PEX14, which mediate docking and assist cargo translocation across the glycosomal/peroxisomal membrane [15–17]. The precise structural details of this translocation process remain incompletely resolved, but PEX14 is well established as a central docking component for the PEX5–cargo complex at the glycosomal/peroxisomal membrane [18]. The structural model used in this work corresponds to *T. cruzi*; however, PEX5–cargo docking through membrane components including PEX13 and PEX14 has also been described in *T. brucei*. More broadly, glycosome biogenesis in trypanosomatids relies on homologous peroxin-dependent import pathways, supporting the relevance of the PEX5–PEX14 interface across *Trypanosoma* species [19, 20].

Because glycosomal protein import depends critically on the PEX5–PEX14 interaction, this protein–protein interface represents a promising target for the development of inhibitors against human trypanosomiases [21, 22]. Despite sustained efforts to identify new antitrypanosomal agents from natural and synthetic products [23, 24], drug repurposing campaigns [25], and alternative chemotherapeutic strategies [26, 27], treatment options remain limited. For Chagas disease, therapy still relies primarily on benznidazole and nifurtimox, drugs introduced several decades ago and associated with limited efficacy, particularly in the chronic phase, as well as frequent adverse effects [28–31]. For HAT, recent therapeutic advances, particularly the introduction and expanded indication of fexinidazole, have improved treatment options for both gambiense and rhodesiense disease. However, therapeutic choice still depends on disease form, stage, age, body weight, drug availability, and treatment setting, with some regimens remaining constrained by toxicity, supervision requirements, or complex administration logistics [32, 33]. New compounds with improved trypanocidal activity, better safety profiles, and alternative mechanisms of action are therefore urgently needed.

In this work, we use molecular docking, molecular dynamics simulations, and free-energy calculations to examine the structural features that shape the PEX5–PEX14 interaction and the binding of small molecules to the PEX14 recognition groove. We first characterise the native PEX5–PEX14 interface and then use the reported inhibitor ET7 as a reference ligand for PEX14 recognition [22]. We subsequently evaluate SuFEx-functionalised naphthoquinones from a previously reported antitrypanosomal series [34, 35] as candidate PEX14-binding scaffolds. These compounds contain a sulfur(VI) fluoride exchange (SuFEx) handle that enables derivatisation at the sulfonyl centre, as discussed in detail in Section 3.3 [36]. Comparison of the native PEX5–PEX14 complex with PEX14-bound small molecules allows us to identify the aromatic, electrostatic, and hydrogen-bonding contacts that stabilise this interface and to assess whether candidate ligands can reproduce key elements of the PEX5 recognition motif. This approach provides a molecular basis for evaluating PEX14-binding scaffolds and supports the development of new inhibitors targeting glycosomal protein import in *Trypanosoma* species.

2 Methods

The crystal structure of the *Trypanosoma cruzi* peroxisomal import assembly reported under Protein Data Bank (PDB) entry 8GI0 [37] was used as the starting model. This structure was selected because it provides an experimentally resolved trypanosomal PEX5–PEX14 interface within a cargo-bound import assembly, containing the cargo enzyme malate dehydrogenase (MDH), full-length PEX5, and the *N*-terminal domain of PEX14. Since the present study focuses on molecular recognition at the PEX5–PEX14 interface and on ligand binding to the PEX14 recognition groove, the MDH cargo was removed and only the PEX5–PEX14 subcomplex was retained. This subcomplex corresponds to chains E and

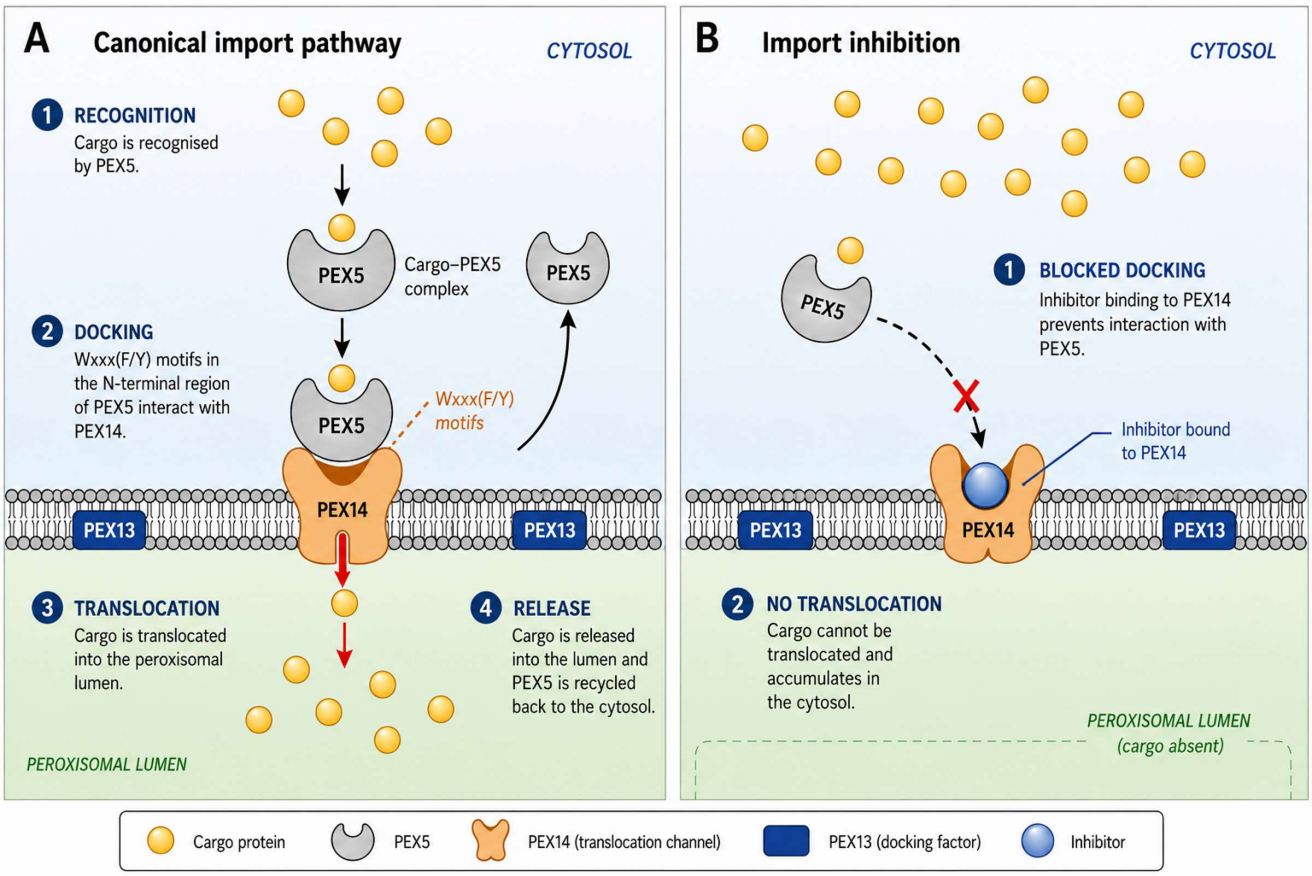


Fig. 1 Peroxisomal/glycosomal protein import and its inhibition. **(A)** In the canonical import pathway, cargo proteins are recognised by the C-terminal domain of PEX5, forming a cargo–PEX5 complex. This complex docks at the peroxisomal/glycosomal membrane, where Wxxx(F/Y) motifs within the N-terminal region of PEX5 interact with PEX14, with PEX13 contributing to the membrane-associated docking and translocation machinery. These interactions enable cargo translocation into the organelle lumen. **(B)** In the presence of an inhibitor, recognition between the cargo–PEX5 complex and PEX14 is blocked, perturbing the docking/translocation process. Consequently, cargo enzymes accumulate in the cytosol, disrupting essential metabolic processes and potentially leading to parasite death.

F of the original crystal structure, respectively. The retained model preserves the PEX14 groove occupied by the canonical PEX5 Wxxx(F/Y) motif and was therefore used both to characterise the native protein–protein interface and to define the ligand-binding region explored in the docking calculations.

Molecular docking of PEX14 with the selected ligands was performed using AutoDock Vina [38, 39]. The PEX14 receptor was extracted from the 8GI0 structure after removal of the MDH cargo and PEX5 chain. Ligand structures were drawn using GaussView 6 [40] and pre-optimised at the ωB97X-D[41]/def2-SVP[42] level of theory using Gaussian 16 [43]. System setup, definition of the search box, and analysis of docking poses were carried out using UCSF Chimera, version 1.19 [44]. The docking box was centred on the PEX14 groove that accommodates the PEX5 Wxxx(F/Y) motif in the native complex, enabling direct comparison between ligand poses and the PEX5 recognition mode. The docking protocol was validated by redocking ET7 into the PEX14 binding site of its crystallographic complex, PDB ID 7QRC [22], after removal of crystallographic water molecules. Docking calculations were performed with an exhaustiveness value of 60, generating nine poses. The search box was centred at $(x, y, z) = (-1.806,\ 12.041,\ 12.684)$ with dimensions of $15.0 \times 17.25 \times 15.0$ Å. The best-ranked redocked pose reproduced the crystallographic ET7 binding mode with an RMSD of 1.221 Å and a docking score of -7.1 kcal mol^{-1}. The same docking parameters were then applied to the 8GI0-derived PEX14 receptor.

Molecular dynamics (MD) simulations of the PEX5–PEX14 complex were performed using the Amber 24 software suite [45, 46] under periodic boundary conditions. The system was prepared using the `tleap` module of AmberTools [47]. The protein was parameterised with the ff14SB force field [48] and solvated in an octahedral periodic box of explicit TIP3P water molecules [49], maintaining a minimum buffer of 10 Å between the solute and the box boundaries. Short-range non-bonded interactions were evaluated using a 10 Å cut-off, while long-range electrostatics were treated using the Particle Mesh Ewald method [50]. Covalent bonds involving hydrogen atoms were constrained using the SHAKE algorithm [51], allowing the use of a 2 fs integration time step.

Energy minimisation was carried out in two stages. First, solvent molecules were minimised while the protein was restrained using a harmonic potential with a force constant of 10.0 kcal mol^{-1} Å^{-2}. This step consisted of 5,000 cycles, including 2,500 steps of steepest descent

followed by 2,500 steps of conjugate-gradient minimisation under constant-volume conditions. In the second stage, all restraints were removed and the entire system was subjected to an additional 5,000 cycles of minimisation using the same protocol. Following minimisation, the system was equilibrated for 20 ps under constant-volume conditions. Initial velocities were assigned from a Maxwell–Boltzmann distribution, and the temperature was gradually increased to 300 K using Langevin dynamics [52] with a collision frequency of 1.0 ps^{-1} while maintaining isotropic pressure at 1 atm. During this stage, weak positional restraints of 10.0 kcal mol^{-1} $Å^{-2}$ were applied to the solute to maintain structural integrity while allowing solvent relaxation.

The equilibrated system was subsequently subjected to three independent 500 ns production MD simulations in the NPT ensemble at 300 K and 1 atm. Temperature was maintained using Langevin dynamics with a collision frequency of 1.0 ps^{-1}, and pressure was regulated using isotropic coupling with a relaxation time of 2.0 ps. No positional restraints were applied during the production stage. Trajectory coordinates and energy data were recorded every 5,000 steps, corresponding to 10 ps, and restart files were saved at regular intervals. Trajectory analysis was performed using CPPTRAJ [53].

Additional MD simulations were performed for PEX14 in complex with the docked ligands. The protein was prepared as described above, and each ligand was placed in the PEX14 recognition groove using the top-ranked docking pose as the initial geometry. For each ligand, `antechamber` [54](AmberTools) was used to prepare a Gaussian 16 input file with the net molecular charge set to zero. Geometry optimisation and evaluation of the molecular electrostatic potential were carried out at the ωB97X-D/def2-SVP level of theory using Gaussian 16, with the electrostatic potential sampled using the Merz–Kollman scheme. Atomic partial charges were then derived by fitting to this potential using the restrained electrostatic potential (RESP) procedure [55] as implemented in `antechamber`, and AMBER atom types were assigned. Missing bonded and van der Waals parameters were generated with `parmchk2`. The protein–ligand complexes were then solvated, minimised, equilibrated, and simulated using the same general MD protocol.

Binding free energies were estimated using the MM–PBSA method [56, 57], as implemented in the `MMPBSA.py` module of AmberTools [58]. Calculations were performed using the final 300 frames extracted from the MD trajectories, sampled every two frames. For the 3L–PEX14 complex, which dissociated during the simulations, MM–PBSA calculations were restricted to the first 100 trajectory frames corresponding to the initially bound portion of the simulation. Solvent molecules and counterions were removed prior to analysis using the mask `:WAT:Na+:Cl-`. Poisson–Boltzmann calculations were carried out with an ionic strength of 0.15 M and the default dielectric constants implemented in Amber, using a solute dielectric constant of 1.0 and a solvent dielectric constant of 80.0. Entropic contributions were not included in the binding free-energy estimates; therefore, the calculated values were interpreted as comparative estimates rather than absolute binding affinities.

3 Results and discussion

3.1 Analysis of the PEX5–PEX14 interface

Figure 2 shows the PEX5–PEX14 subcomplex extracted from the *T. cruzi* peroxisomal import assembly used in this study. In this structure, PEX5 binds to the *N*-terminal domain of PEX14 through an α-helical segment that lies across a shallow hydrophobic groove on the PEX14 surface. The main PEX14-binding sequence of PEX5 corresponds to residues Trp60–Val61–Arg62–Glu63–Tyr64, hereafter referred to as the 60–WVREY–64 motif. This sequence matches the canonical Wxxx(F/Y) pattern involved in PEX14 recognition, in which the first and last positions are occupied by aromatic residues. The motif forms part of an α-helix extending from Glu59 to Glu76, positioning Trp60 and Tyr64 directly within the PEX14 recognition groove.

The shape of this groove is largely defined by two closely positioned, π-stacked phenylalanine residues, Phe12 and Phe29, which divide the binding surface into two shallow hydrophobic cavities (Figure 2). This structural arrangement creates a compact aromatic environment in which the side chains of Trp60 and Tyr64 from PEX5 can establish stabilising contacts with PEX14. In addition to this canonical binding region, a second PEX5 segment, residues 86–NNPYMY–90, is located close to the PEX14 surface in the starting structure. This secondary region contains Tyr residues that may also contribute to transient aromatic contacts with PEX14 during the simulations. Together, the 60–WVREY–64 motif, the neighbouring 86–NNPYMY–90 region, and the PEX14 residues Phe12, Phe29, Thr21, and Lys33 define the interaction region analysed throughout the MD trajectories.

This structural arrangement provides a reference for interpreting both the native PEX5–PEX14 interaction and the binding modes of the small molecules investigated below. In particular, the position of Trp60 and Tyr64 within the PEX14 groove identifies the regions that candidate ligands would need to occupy to mimic the native PEX5 recognition motif. The same groove was therefore used as the target region for molecular docking, and the persistence of aromatic, electrostatic, and hydrogen-bonding contacts within this region was monitored during the MD simulations.

Our MD simulations revealed that PEX5 and PEX14 remained associated over 500 ns in the three independent replicas, despite localised flexibility at the terminal regions (Figure S1). Binding free energy estimates derived from MM–PBSA calculations yielded an average value of -16.56 ± 0.66 kcal mol^{-1} (Table S1), consistent with a stable protein–protein complex. These values should nevertheless be interpreted qualitatively, as comparative estimates rather than absolute binding affinities.

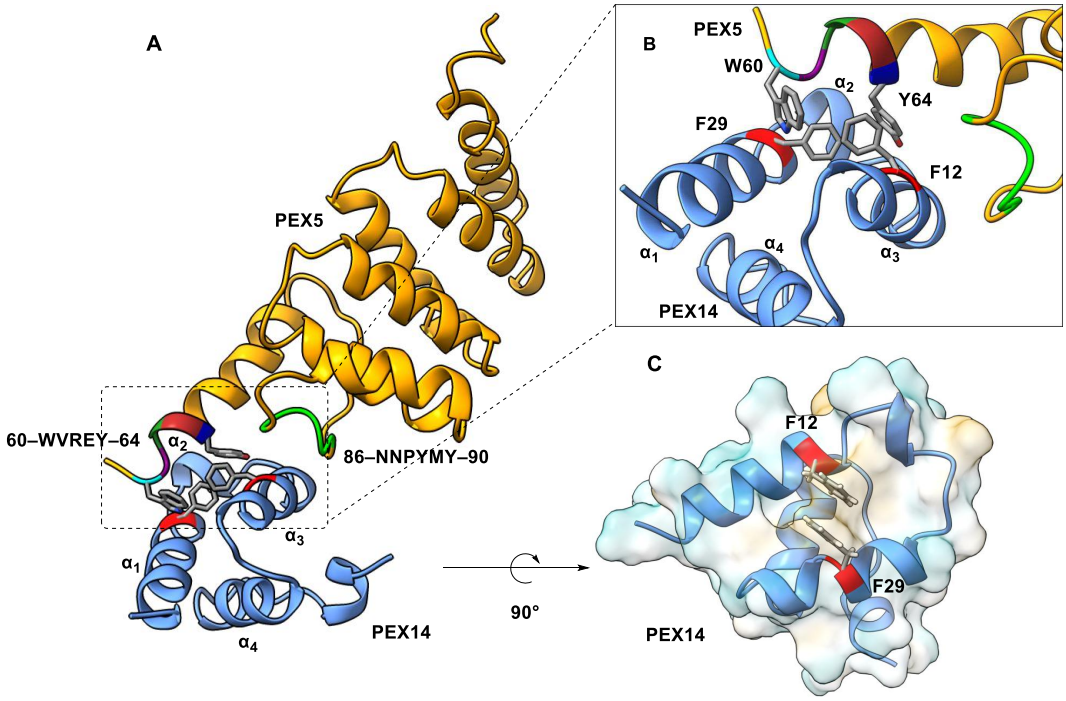


Fig. 2 PEX5–PEX14 complex. **(A)** PEX5 is shown in yellow, with the 60–WVREY–64 motif highlighted in red, PEX14 in blue, and the secondary 86–NNPYMY–90 region in green. **(B)** Close-up of the primary PEX5–PEX14 interface, highlighting Trp60 and Tyr64 of PEX5 in red, and Phe12 and Phe29 of PEX14 in blue. **(C)** Top view of PEX14 showing the cavity divided by Phe12 and Phe29.

Trajectory analysis confirmed that the interaction is centred on the canonical 60–WVREY–64 motif, while also involving contacts from the secondary 86–NNPYMY–90 region, in agreement with the structural heterogeneity reported for the peroxisomal import complex [37] (Figure S3). The contribution of both regions supports a multivalent recognition mode, in which PEX14 binding is maintained through several contacts distributed across the *N*-terminal region of PEX5 rather than through a single static interaction.

Figure 3 summarises representative contacts observed during the MD simulations. Panels **A** and **B** show the relative orientation of the PEX5 Wxxx(F/Y) motif and the PEX14 groove, highlighting the proximity of Trp60 and Tyr64 to the aromatic residues Phe12 and Phe29. This arrangement places the canonical PEX5 motif in a position suitable for simultaneous electrostatic, hydrogen-bonding, and aromatic interactions with PEX14.

At the residue level, the spatial arrangement of Trp60 and Glu63 in PEX5 enables simultaneous interactions with Lys33 of PEX14. Trp60 engages in a π–cation interaction with Lys33, while Glu63 forms a salt bridge with the same residue (Figure 3**C** and Table S1). Hydrogen bonding also contributes to the stability of the complex, particularly through the interaction between Tyr64 and Thr21, which was among the most persistent contacts observed throughout the simulations (Figure 3**D** and Figure S3). Other frequently sampled hydrogen bonds include Asn85–Gln28, Gln68–Asn25, and Pro87–Ser32, further supporting the presence of an extended interaction network involving both the canonical motif and the neighbouring PEX5 region.

Aromatic interactions also make an important contribution to the stability of the PEX5–PEX14 complex. T-shaped edge-to-face contacts were consistently observed for residues belonging to both the canonical 60–WVREY–64 motif and the secondary 86–NNPYMY–90 region. In the canonical binding region, Tyr64 of PEX5 forms a T-shaped interaction with Phe12 of PEX14 (Figure 3**F**), whereas in the secondary region Tyr90 forms an analogous contact with Phe29 (Figure 3**E**). The persistence of these interactions across the trajectories indicates that both PEX5 regions participate in stabilising contacts with the PEX14 groove (Table S1). Together with the hydrogen bonds, salt bridges, and π–cation contacts described above, these results support a model in which PEX5–PEX14 association is maintained by canonical Wxxx(F/Y) motif recognition reinforced by additional transient contacts distributed across neighbouring PEX5 segments. This picture is consistent with the conformational heterogeneity reported for the peroxisomal import complex [37] and highlights the dynamic and multivalent character of the PEX5–PEX14 interface.

3.2 ET7 as a reference ligand for PEX14 recognition

To establish a reference for small-molecule recognition of the PEX14 groove, we first examined N-(5-ethyl-6-oxidanylidene-benzo[b][1,4]benzothiazepin-2-yl)-2-(4-fluorophenyl)ethanamide, hereafter referred

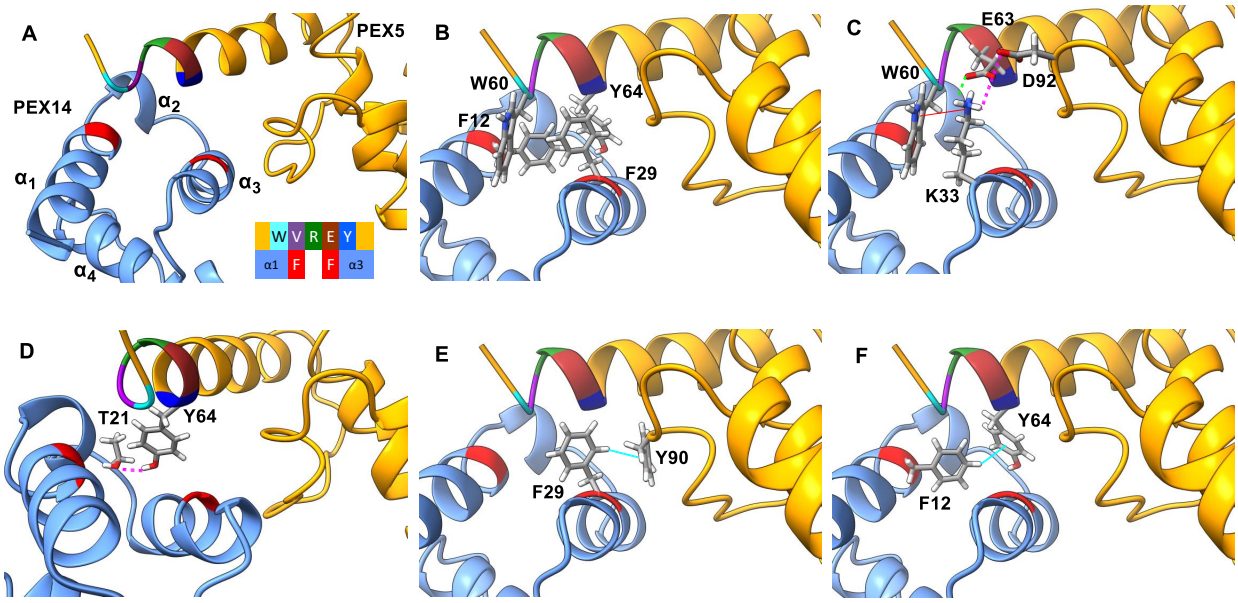


Fig. 3 Interactions observed during 500 ns MD simulations across three replicas. **(A)** PEX5 (yellow) and PEX14 (light blue), with the Wxxx(F/Y) motif highlighted: Trp (cyan), Val (purple), Arg (dark green), Glu (brown), and Tyr (dark blue). PEX14 residues Phe12 and Phe29 are shown in red. **(B)** Interactions of PEX5 Trp60 and Tyr64 with PEX14 Phe12 and Phe29. **(C)** Simultaneous interactions between Lys33 and PEX5 residues: a salt bridge with Glu63 (light green dashed line) and a π–cation interaction with Trp60 (red line). **(D)** Hydrogen bond between Thr21 and Tyr64 (magenta dashed line). **(E)** T-shaped π interaction between Phe29 and Tyr90. **(F)** T-shaped π interaction between Phe12 and Tyr64.

to as ET7, a previously reported inhibitor of the PEX5–PEX14 interaction (PDB ID: 7QRC [22]). ET7 (Figure 4**A**) was developed through a structure-based drug-design strategy targeting the PEX5–PEX14 interface in *T. cruzi*. It was designed to disrupt recognition of the conserved Wxxx(F/Y) motifs of PEX5 by the *N*-terminal domain of PEX14. In the present work, ET7 was used as a reference ligand because its experimental PEX14-bound structure allows direct comparison between the crystallographic binding mode, the docking results, and the MD simulations.

The discovery of ET7 originated from a high-throughput AlphaScreen assay aimed at identifying inhibitors of the PEX5–PEX14 protein–protein interaction (PPI). This was followed by orthogonal validation using saturation transfer difference NMR (STD-NMR), which confirmed direct binding to PEX14 and ruled out assay artefacts. Subsequent structural characterisation of the PEX14–ligand complex, together with structure–activity relationship (SAR) studies, enabled the refinement of ET7 into an optimised derivative with improved binding affinity and trypanocidal activity. ET7 was therefore not only validated as a PEX14-binding inhibitor, but also proposed as a promising scaffold for the development of a new class of trypanocidal compounds targeting the essential PEX5–PEX14 interaction pathway.

The ET7 ligand was extracted from its crystallographic complex with PEX14 (PDB ID: 7QRC) and optimised at the ωB97X-D/def2-SVP level of theory. To validate the docking protocol, ET7 was first redocked into the PEX14 binding site of the 7QRC crystal structure after removal of all crystallographic water molecules. Following validation, molecular docking calculations were performed using the PEX14 receptor extracted from the 8GI0 crystal structure employed throughout this study, applying the same docking-box parameters used in the redocking procedure. This allowed the ET7 binding mode predicted for the 8GI0-derived PEX14 model to be compared directly with both the crystallographic ET7 pose and the native PEX5 recognition mode. The main structural difference between the 7QRC and 8GI0 PEX14 models is the presence of the first three amino acids, Ser1, Ser2, and Glu3, in 7QRC, which are absent in 8GI0. All docking poses and corresponding binding free energies are reported in Figure S4.

After validating the docking protocol against the crystallographic ET7–PEX14 complex from 7QRC, the same procedure was applied to the PEX14 receptor extracted from the 8GI0 structure used throughout this study. In this 8GI0-derived model, the top-ranked ET7 pose showed a predicted docking score of -6.4 kcal mol^{-1}. The 4-fluorophenyl moiety of ET7 is oriented toward Lys33 of PEX14 (Figure 4**D**), occupying a region that overlaps with the Trp60-binding site of PEX5 (Figure 4**G**). This binding mode is consistent with the crystallographic pose observed in 7QRC, for which the redocking validation gave a score of -7.1 kcal mol^{-1} and an RMSD of 1.221 Å. The dibenzo[b,f][1,4]thiazepin-11(10H)-one core, in turn, extends toward the region occupied by Tyr64 in the native PEX5–PEX14 complex. This arrangement places both aromatic portions of ET7 close to Phe12 and Phe29, favouring T-shaped π interactions with the PEX14 groove, while the proximity of the 4-fluorophenyl group to Lys33 is compatible with a π–cation contact.

To evaluate the stability of the docking-predicted ET7 binding mode, MD simulations were performed starting from the top-ranked docking pose. These simulations

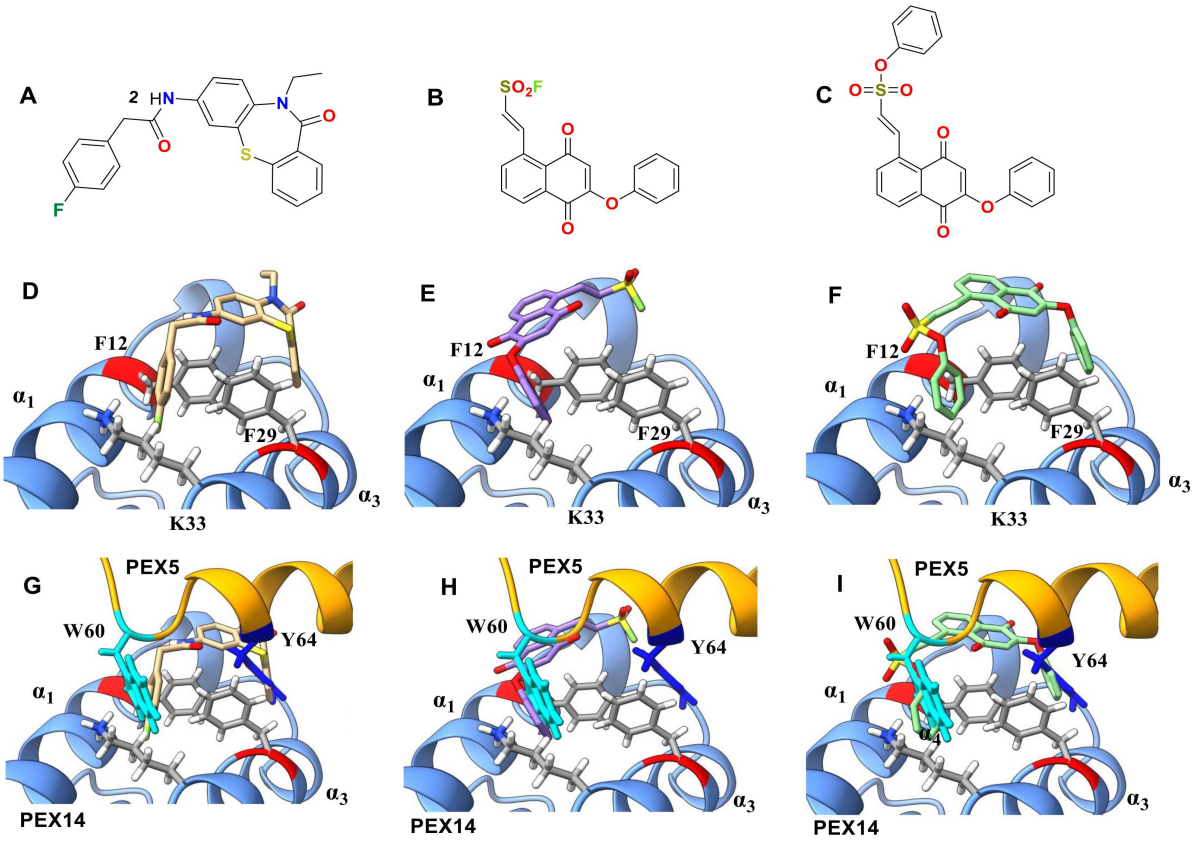


Fig. 4 Molecular docking results. Chemical structures of the ligands ET7 **(A)**, 3L **(B)**, and 3L-OAr **(C)**. Top-ranked docking poses of ET7 **(D)**, 3L **(E)**, and 3L-OAr **(F)** within the PEX14 binding groove. Superposition of ET7 **(G)**, 3L **(H)**, and 3L-OAr **(I)** with the PEX5–PEX14 complex, shown alongside PEX5.

allowed us to assess whether the key contacts identified from docking, particularly T-shaped aromatic and π–cation interactions, were maintained over time under explicit-solvent conditions. MM–PBSA calculations were then used to estimate the relative binding free energy of the ET7–PEX14 complex.

The MD simulations showed that ET7 remained predominantly within the 60–WVREY–64 binding region of PEX14 throughout the trajectories (Figure S7 and Figure S10). Across the three replicas, the 4-fluorophenyl group consistently occupied the Trp60 pocket, whereas the dibenzo[b,f][1,4]thiazepin scaffold localised near the Tyr64 region. This arrangement effectively shields Phe12 and Phe29 and is in agreement with previous structural observations for the ET7–PEX14 complex [22].

The main ET7–PEX14 contacts identified during the simulations are shown in Figure 5. These include T-shaped aromatic interactions with Phe12 and Phe29, a π–cation contact with Lys33, and a hydrogen bond involving Asp15. The bent geometry of the dibenzo[b,f][1,4]thiazepin scaffold allows the eastern benzene ring of ET7 (Figure 4A) to engage simultaneously in distinct T-shaped π interactions with both phenylalanine residues. Specifically, a face-to-edge interaction is observed with Phe29, in which the aromatic face of Phe29 contacts the edge of the ligand ring (Figure 5**A**). In contrast, Phe12 interacts in the opposite orientation, with its edge contacting the aromatic face of ET7 (Figure 5**B**). Across the three independent MD replicas, $\text{Phe29}_{\text{face}}$–$\text{ET7}_{\text{edge}}$ interactions occurred with frequencies between 23.86% and 43.64%, whereas ET7_{face}–$\text{Phe12}_{\text{edge}}$ interactions ranged from 21.16% to 40.48% (Table S2).

In addition to these aromatic contacts, a π–cation interaction between Lys33 and the 4-fluorophenyl group was observed, with occupancies between 16.88% and 39.22% across the trajectories (Figure 5**C**). Notably, in Run 2, where T-shaped interactions were most frequent and π–cation contacts least prevalent, hydrogen bonding between Asp15 and the 4-fluorophenylacetamide moiety became dominant (Figure S11). This interaction shifts the ligand toward the α2 helix, reducing its proximity to Lys33 and thereby disfavouring π–cation formation (Figure 5**D**). Consistent with the sustained residence of ET7 within the PEX14 groove and the persistence of these interaction patterns, MM–PBSA analysis yielded an average binding free energy of -5.45 ± 1.36 kcal mol^{-1}, supporting the formation of a moderately stable ligand–protein complex.

3.3 SuFEx-functionalised naphthoquinones as PEX14-binding candidates

Sulfur(VI) fluoride exchange (SuFEx) chemistry is a chemoselective click-chemistry platform based on the controlled exchange of sulfur(VI)–fluoride bonds. In medicinal chemistry, SuFEx is attractive because sulfonyl

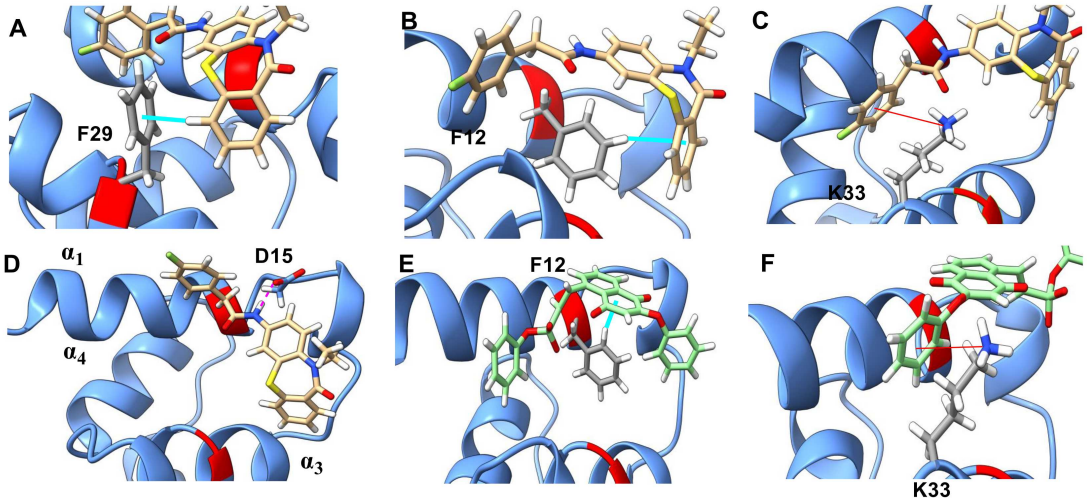


Fig. 5 Representative interactions between PEX14 and the ET7 and 3L-OAr ligands observed during MD simulations. **(A)** T-shaped interaction between the aromatic face of Phe29 and the edge of ET7. **(B)** T-shaped interaction between the aromatic face of ET7 and the edge of Phe12. **(C)** π–cation interaction between the 4-fluorophenyl moiety of ET7 and Lys33. **(D)** Hydrogen bond between Asp15 and the NH group of the 4-fluorophenylacetamide moiety of ET7. **(E)** T-shaped interaction between the aromatic face of 3L-OAr and the edge of Phe12. **(F)** π–cation interaction between the aryl sulfonate moiety of 3L-OAr and Lys33. T-shaped interactions are shown as cyan lines, π–cation interactions as red lines, and hydrogen bonds as magenta dashed lines.

fluorides, fluorosulfates, and related sulfur(VI) fluorides can be converted into sulfur(VI)-containing derivatives such as sulfonates, sulfonamides, and related motifs, providing access to modular and often metabolically robust functionalities [36, 59, 60]. This reactivity is particularly useful for late-stage diversification, as it enables new substituents to be introduced into bioactive scaffolds without requiring complete redesign of the molecular framework. Recent work has further highlighted the therapeutic potential of SuFEx-based compounds, including the development of the aryl fluorosulfate antitubercular candidate CMX410, which irreversibly inhibits the essential *Mycobacterium tuberculosis* enzyme Pks13 [61].

SuFEx-functionalised naphthoquinones were therefore considered as potential PEX14-binding ligands. The relevance of this molecular platform is further supported by the broader medicinal chemistry of quinones, which are privileged redox-active scaffolds owing to their structural diversity, reversible redox chemistry, and ability to form covalent adducts [62–64]. These features have been associated with broad biological activity, including anticancer, antimicrobial, antiparasitic, and anti-inflammatory effects [65–67]. In the context of neglected tropical diseases, naphthoquinones are particularly attractive because selective functionalisation of the quinoidal framework can tune electronic structure, redox properties, and molecular-recognition features relevant to antiparasitic activity [68, 69].

Although the trypanocidal activity of naphthoquinones is commonly associated with redox cycling, mitochondrial dysfunction, and reactive oxygen species (ROS) generation [70–73], their potential to act as PPI inhibitors is much less established in the context of trypanosomatid drug discovery. Nevertheless, quinone-containing scaffolds have been reported as modulators of PPIs in other biological systems, including the X-linked inhibitor of apoptosis protein (XIAP) [74], the Kelch-like ECH-associated protein 1–nuclear factor erythroid 2-related factor 2 (Keap1–Nrf2) interface [75], the Yes-associated protein–TEA domain transcription factor (YAP–TEAD) interface [76], and the hypoxia-inducible factor 1α–p300/CREB-binding protein (HIF-1α–p300/CBP) interface [77]. In the Chagas disease context, recent in silico work on lapachol derivatives has also combined PPI network analysis with molecular docking, identifying heat shock protein 90 (HSP90) as a potential target for naphthoquinone-based ligand design [78]. These examples suggest that naphthoquinone derivatives may be explored not only as redox-active trypanocidal agents, but also as scaffolds for targeting defined recognition surfaces such as the PEX14 groove.

A recently reported Ru-catalysed C–H alkenylation strategy enabled the installation of an ethenesulfonyl fluoride group at the C-5 position of the naphthoquinone A-ring, furnishing SuFEx-ready naphthoquinone derivatives with antitrypanosomal activity against *T. cruzi* [34, 35]. Importantly, several compounds from this series displayed significant trypanocidal activity against *T. cruzi*, highlighting the potential of this synthetic platform for the development of new therapeutic candidates against neglected tropical diseases such as Chagas disease. The presence of the sulfonyl fluoride group is especially relevant for the present study because it provides a direct point for SuFEx derivatisation, enabling the introduction of additional aromatic substituents that may improve complementarity with the aromatic and electrostatic environment of the PEX14 binding groove.

Based on the interaction pattern identified for the native PEX5–PEX14 complex and the ET7 reference ligand, we next evaluated whether SuFEx-functionalised naphthoquinones could occupy the PEX14 recognition groove and reproduce key elements of the PEX5 binding mode. The compounds were analysed using the

same computational workflow described above, comprising molecular docking, MD simulations, and MM–PBSA binding free-energy calculations. This allowed comparison of their binding poses, interaction profiles, residence within the PEX14 groove, and potential overlap with the PEX5–PEX14 interface.

Among the compounds in the previously reported series [34], 3L (Figure 4B) was selected as a representative ligand for the present analysis. This choice was motivated by the presence of a phenyl substituent, which could favour aromatic contacts with residues lining the PEX14 binding groove, including π–π, π–cation, and T-shaped interactions. Although 3L was not the most active derivative against *T. cruzi*, its trypanocidal activity was comparable to that of benznidazole, making it a relevant starting point for assessing whether SuFEx-functionalised naphthoquinones can mimic key features of the PEX5 recognition mode at the PEX14 interface.

The top-ranked docking pose of 3L gave a predicted docking score of -6.2 kcal mol^{-1} (Figure S5). In this pose, the 1,4-naphthoquinone core occupies the region surrounding Phe12, adopting an orientation compatible with a stabilising T-shaped aromatic interaction. At the same time, the phenyl substituent is positioned close to Lys33 in a geometry suitable for a π–cation interaction (Figure 4**E**). This binding arrangement reproduces key interaction features observed for both the native PEX5 Wxxx(F/Y) motif and the ET7 reference ligand (Figure 4**H**), suggesting that 3L may partially mimic the PEX5 recognition mode at the PEX14 binding groove.

This binding geometry was maintained for approximately the first 50 ns of the MD simulations, indicating an initially favourable recognition mode. However, as the trajectories progressed, 3L gradually drifted away from the PEX14 groove and eventually dissociated from the protein interaction site. Trajectory analysis also revealed only a limited number of persistent hydrogen-bond interactions (Figure S12). These results suggest that, although the docking pose captures favourable early recognition features, the 3L–PEX14 complex lacks the stability required to sustain persistent binding under dynamic conditions. Consistent with this interpretation, MM–PBSA calculations performed over the first 100 trajectory frames, corresponding exclusively to the initially bound portion of the simulation, yielded an average binding free energy of merely -1.43 ± 2.05 kcal mol^{-1} (Table S3). This weakly favourable value further supports the transient nature of the interaction.

As a preliminary optimisation strategy to improve ligand recognition by PEX14, an in silico SuFEx-derived analogue of 3L was generated by replacing the fluorine atom of the ethenesulfonyl fluoride group with a phenoxy substituent. This modification, inspired by previously reported SuFEx derivatisation approaches [36], converts the sulfonyl fluoride motif into an aryl sulfonate while introducing an additional aromatic group. The resulting analogue, here designated 3L-OAr (Figure 4**C**), was then evaluated using the same computational workflow to assess whether this added aromatic substituent could strengthen stabilising interactions within the PEX14 binding groove.

The additional aromatic substituent in 3L-OAr was associated with improved predicted ligand–protein recognition, as indicated by a more favourable docking score of -7.03 kcal mol^{-1} relative to 3L (Figure S6). In the top-ranked docking pose, the aryl sulfonate motif occupies the Trp60 pocket (Figure 4**F**,**I**), placing the added aromatic ring in a region that overlaps with the native PEX5 recognition motif. In all three independent MD simulations, 3L-OAr remained associated with the 60–WVREY–64 binding region for substantially longer periods than 3L. Consistent with this increased residence within the PEX14 groove, MM–PBSA calculations yielded an improved average binding free energy of -4.04 ± 1.16 kcal mol^{-1} (Table S4).

The most frequent interaction observed across the 500 ns MD simulations was a T-shaped aromatic contact between the face of the 1,4-naphthoquinone moiety of 3L-OAr and the edge of Phe12 (Figure 5**E** and Table S4). A second recurrent interaction was a π–cation contact between the aryl ether fragment of 3L-OAr, corresponding to fragment 2 in Figure 4**C**, and Lys33 (Figure 5**F** and Table S4). These contacts are consistent with the intended role of the added aromatic substituent, which extends ligand recognition into the Trp60 pocket while maintaining aromatic stabilisation near Phe12.

A modest improvement in hydrogen-bonding interactions was also observed (Figure S13). Although hydrogen bonds involving the oxygen atoms of the aryl sulfonate group were detected only intermittently throughout the trajectories, their presence suggests that this region may contribute to ligand stabilisation within the PEX14 binding groove. Because both 3L and 3L-OAr contain only hydrogen-bond acceptor functionalities, the incorporation of hydrogen-bond donor groups, together with a carefully controlled increase in ligand size, may represent a promising strategy for further improving predicted binding strength, residence within the PEX14 groove, and complementarity with the PEX14 interaction interface.

4 Conclusion

In this work, we employed an integrated computational strategy combining molecular docking, molecular dynamics simulations, and MM–PBSA free-energy calculations to examine the structural features that stabilise the PEX5–PEX14 interaction and mediate small-molecule recognition at the PEX14 groove. Because the PEX5–PEX14 interface is essential for glycosomal protein import in trypanosomatids, defining the interaction patterns that support this association is relevant for the rational development of new antitrypanosomal agents.

Our analyses revealed that the PEX5–PEX14 complex is stabilised by a dynamic and multivalent interaction network involving not only the canonical Wxxx(F/Y) motif but also secondary interaction regions. In particular, aromatic contacts, especially T-shaped interactions involving Phe12 and Phe29 of PEX14,

together with hydrogen bonds and electrostatic interactions centred around Lys33, emerged as key contributors to complex stability. These findings reinforce the importance of aromatic recognition and transient intermolecular contacts in maintaining the PEX5–PEX14 association.

The investigation of the ET7 reference inhibitor further demonstrated that successful occupation of the PEX14 groove relies on the ability of ligands to reproduce these stabilising interaction patterns. ET7 remained associated with the binding groove throughout the simulations and established persistent T-shaped interactions and π–cation contacts, supporting its role as a validated scaffold capable of mimicking essential features of the native PEX5 recognition motif.

Evaluation of the SuFEx-functionalised naphthoquinone derivative 3L showed that, although the compound initially adopts a binding pose compatible with PEX5-like recognition within the PEX14 groove, the complex is not sufficiently stabilised to sustain persistent binding under dynamic conditions. In contrast, in silico SuFEx derivatisation of 3L through replacement of the sulfonyl fluoride fluorine atom with a phenoxy substituent generated the aryl sulfonate analogue 3L-OAr, which displayed an improved docking score, longer residence within the PEX14 groove, and a more favourable MM–PBSA binding free energy. These improvements were associated with increased aromatic complementarity, particularly through recurrent T-shaped interactions with Phe12 and π–cation interactions with Lys33.

These results identify aromatic and electrostatic contacts as central features for ligand stabilisation at the PEX14 interface and support SuFEx-derived naphthoquinones as promising scaffolds for further optimisation as PEX14-binding candidates. Future ligand design should consider the introduction of hydrogen-bond donor groups, together with a controlled increase in ligand size, to improve predicted binding strength, residence within the PEX14 groove, and complementarity with the PEX5 recognition region. This study provides a structural framework for the rational, function-driven design of new ligands targeting glycosomal protein import, guided by a computational protocol that focuses on the specific interactions underlying protein function, and reinforces PEX14 as a promising molecular target for therapeutic development against diseases such as Chagas disease and human African trypanosomiasis.

Supplementary information. The Supplementary Information contains additional analyses supporting the MD, docking, and MM–PBSA results discussed in the main text. These include RMSD profiles for the PEX5–PEX14, ET7–PEX14, 3L–PEX14, and 3L-OAr–PEX14 simulations; residue-contact and hydrogen-bond analyses for the PEX5–PEX14 complex; molecular docking poses for ET7, 3L, and 3L-OAr; ligand trajectory mapping on the PEX14 surface; hydrogen-bond time series for the ligand–PEX14 complexes; MM–PBSA binding free energies and interaction percentages for T-shaped aromatic and π–cation contacts; and the optimised Cartesian coordinates of ET7, 3L, and 3L-OAr.

Acknowledgements. This work was supported by the Royal Society ISPF International Collaboration Awards 2024 (Brazil and South Africa), grant No. ICAO\R1\241112, through the NUBIAN project. Additional funding was provided by grant PID2023-151549NB-I00, funded by MICIU/AEI/10.13039/501100011033 and FEDER/UE; grant IT1553-22, funded by the Basque Government; grant I+D+i/CEX2024-001491-S, funded by MICIU/AEI/10.13039/501100011033 through the Spanish Severo Ochoa Centre of Excellence programme; and grant TRNSC259889COSS, funded by the Fundación Científica de la Asociación Española Contra el Cáncer under the framework of the ERA-NET TRANSCAN-3 initiative. The authors acknowledge the technical support provided by the Donostia International Physics Center (DIPC) Supercomputing Center. Computational resources were provided by the Hyperion cluster at DIPC. The authors also acknowledge the specialist and high-performance computing systems provided by Information Services at the University of Kent. F.F. acknowledges support from the Marie Skłodowska-Curie Actions under Grant Agreement Nos. 101299799 and 101225527, and from the Royal Society of Chemistry Inclusion and Diversity Fund under Grant No. 280026109.

Conflict of interest

The authors declare no competing interests.

Data availability

The data supporting the findings of this study are available within the article and its Supplementary Information. Additional simulation input files and analysed trajectory data are available from the corresponding author upon reasonable request.

Author contributions

A.R.G.: Conceptualisation, methodology, software, formal analysis, investigation, data curation, writing – original draft, writing – review and editing, visualisation. **E.R.S.P.:** Validation, writing – review and editing. **A.S.-T.:** Validation, writing – review and editing. **C.H.-A.:** Validation, writing – review and editing. **I.R.:** Methodology, resources, writing – review and editing. **O.R.B.:** Resources, writing – review and editing. **C.R.K.:** Validation, writing – review and editing. **G.A.M.J.:** Resources, funding acquisition, writing – review and editing. **E.N.S.J.:** Resources, writing – review and editing. **F.F.:** Conceptualisation, methodology, resources, writing – original draft, writing – review and editing, supervision, project administration, funding acquisition.

References

[1] Barrett, M.P., Burchmore, R.J.S., Stich, A., Lazzari, J.O., Frasch, A.C., Cazzulo, J.J., Krishna, S.: The trypanosomiases. The Lancet **362**, 1469–1480 (2003) https://doi.org/10.1016/S0140-6736(03)14694-6

[2] Langousis, G., Hill, K.L.: Motility and more: the flagellum of trypanosoma brucei. Nature Reviews Microbiology **12**, 505–518 (2014) https://doi.org/10.1038/nrmicro3274

[3] Stuart, K., Brun, R., Croft, S., Fairlamb, A., Gürtler, R.E., McKerrow, J., Reed, S., Tarleton, R.: Kinetoplastids: related protozoan pathogens, different diseases. The Journal of Clinical Investigation **118**, 1301–1310 (2008) https://doi.org/10.1172/JCI33945

[4] Miles, M.A., Feliciangeli, M.D., Arias, A.R.: American trypanosomiasis (chagas' disease) and the role of molecular epidemiology in guiding control strategies. BMJ **326**, 1444–1448 (2003) https://doi.org/10.1136/bmj.326.7404.1444

[5] Kioy, D., Jannin, J., Mattock, N.: Focus: Human african trypanosomiasis. Nature Reviews Microbiology **2**, 186–187 (2004) https://doi.org/10.1038/nrmicro848

[6] Acosta, H., Burchmore, R., Naula, C., Gualdrón-López, M., Quintero-Troconis, E., Cáceres, A.J., Michels, P.A.M., Concepción, J.L., Quiñones, W.: Proteomic analysis of glycosomes from trypanosoma cruzi epimastigotes. Molecular and Biochemical Parasitology **229**, 62–74 (2019) https://doi.org/10.1016/j.molbiopara.2019.02.008

[7] Michels, P.A.M., Hannaert, V., Bringaud, F.: Metabolic aspects of glycosomes in trypanosomatidae – new data and views. Parasitology Today **16**, 482–489 (2000) https://doi.org/10.1016/S0169-4758(00)01810-X

[8] Opperdoes, F.R., Borst, P.: Localization of nine glycolytic enzymes in a microbody-like organelle in trypanosoma brucei: The glycosome. FEBS Letters **80**, 360–364 (1977) https://doi.org/10.1016/0014-5793(77)80476-6

[9] Gatto, G.J., Geisbrecht, B.V., Gould, S.J., Berg, J.M.: Peroxisomal targeting signal-1 recognition by the tpr domains of human pex5. Nature Structural Biology **7**, 1091–1095 (2000) https://doi.org/10.1038/81930

[10] Sampathkumar, P., Roach, C., Michels, P.A.M., Hol, W.G.J.: Structural insights into the recognition of peroxisomal targeting signal 1 by trypanosoma brucei peroxin 5. Journal of Molecular Biology **381**, 867–880 (2008) https://doi.org/10.1016/j.jmb.2008.05.089

[11] Wang, J.-Y., Li, L., Chai, R.-Y., Qiu, H.-P., Zhang, Z., Wang, Y.-L., Liu, X.-H., Lin, F.-C., Sun, G.-C.: Pex13 and pex14, the key components of the peroxisomal docking complex, are required for peroxisome formation, host infection and pathogenicity-related morphogenesis in magnaporthe oryzae. Virulence **10**, 292–314 (2019) https://doi.org/10.1080/21505594.2019.1598172

[12] Lanyon-Hogg, T., Warriner, S.L., Baker, A.: Getting a camel through the eye of a needle: the import of folded proteins by peroxisomes. Biology of the Cell **102**, 245–263 (2010) https://doi.org/10.1042/BC20090159

[13] Thoms, S.: Import of proteins into peroxisomes: piggybacking to a new home away from home. Open Biology **5**, 150148 (2015) https://doi.org/10.1098/rsob.150148

[14] Gabay-Maskit, S., Cruz-Zaragoza, L.D., Shai, N., Eisenstein, M., Bibi, C., Cohen, N., Hansen, T., Yifrach, E., Harpaz, N., Belostotsky, R., Schliebs, W., Schuldiner, M., Erdmann, R., Zalckvar, E.: A piggybacking mechanism enables peroxisomal localization of the glyoxylate cycle enzyme mdh2 in yeast. Journal of Cell Science **133**, 244376 (2020) https://doi.org/10.1242/jcs.244376

[15] Ghosh, M., Denkert, N., Reuter, M., Klümper, J., Reglinski, K., Peschel, R., Schliebs, W., Erdmann, R., Meinecke, M.: Dynamics of the translocation pore of the human peroxisomal protein import machinery. Biological Chemistry **404**(2-3), 169–178 (2023) https://doi.org/10.1515/hsz-2022-0170

[16] Gao, Y., Skowyra, M.L., Feng, P., Rapoport, T.A.: Protein import into peroxisomes occurs through a nuclear pore–like phase. Science **378**, 3971 (2022) https://doi.org/10.1126/science.adf3971

[17] Meinecke, M., Cizmowski, C., Schliebs, W., Krüger, V., Beck, S., Wagner, R., Erdmann, R.: The peroxisomal importomer constitutes a large and highly dynamic pore. Nature Cell Biology **12**, 273–277 (2010) https://doi.org/10.1038/ncb2027

[18] Saidowsky, J., Dodt, G., Kirchberg, K., Wegner, A., Nastainczyk, W., Kunau, W.-H., Schliebs, W.: The di-aromatic pentapeptide repeats of the human peroxisome import receptor pex5 are separate high affinity binding sites for the peroxisomal membrane protein pex14*. Journal of Biological Chemistry **276**, 34524–34529 (2001) https://doi.org/10.1074/jbc.M104647200

[19] Moyersoen, J., Choe, J., Fan, E., Hol, W.G.J., Michels, P.A.M.: Biogenesis of peroxisomes and glycosomes: trypanosomatid glycosome assembly is a promising new drug target. FEMS Microbiol. Rev. **28**(5), 603–643 (2004) https://doi.org/10.1016/j.femsre.2004.06.004

[20] Crowe, L.P., Wilkinson, C.L., Nicholson, K.R., Morris, M.T.: Trypanosoma brucei Pex13.2 is an accessory peroxin that functions in the import of peroxisome targeting sequence type 2 proteins and localizes to subdomains of the glycosome. mSphere **5**(1), 00744–19 (2020) https://doi.org/10.1128/mSphere.00744-19

[21] Dawidowski, M., Emmanouilidis, L., Kalel, V.C., Tripsianes, K., Schorpp, K., Hadian, K., Kaiser, M., Mäser, P., Kolonko, M., Tanghe, S., Rodriguez, A., Schliebs, W., Erdmann, R., Sattler, M., Popowicz, G.M.: Inhibitors of pex14 disrupt protein import into glycosomes and kill trypanosoma parasites. Science **355**, 1416–1420 (2017) https://doi.org/10.1126/science.aal1807

[22] Napolitano, V., Mróz, P., Marciniak, M., Kalel, V.C., Softley, C.A., Olmos, J.D.J., Tippler, B.G., Schorpp, K., Rioton, S., Fröhlich, T., Plettenburg, O., Hadian, K., Erdmann, R., Sattler, M., Popowicz, G.M., Dawidowski, M., Dubin, G.: Structure-based design, synthesis and evaluation of a novel family of pex5-pex14 interaction inhibitors against trypanosoma. European Journal of Medicinal Chemistry **243**, 114778 (2022) https://doi.org/10.1016/j.ejmech.2022.114778

[23] O. Salas, C., Faundez, M., Morello, A., Diego Maya, J., A. Tapia, R.: Natural and Synthetic Naphthoquinones Active Against Trypanosoma Cruzi: An Initial Step Towards New Drugs for Chagas Disease. Curr. Med. Chem. **18**(1), 144–161 (2011) https://doi.org/10.2174/092986711793979779

[24] da Silva Júnior, E.N., Jardim, G.A.M., Jacob, C., Dhawa, U., Ackermann, L., Castro, S.L.: Synthesis of quinones with highlighted biological applications: A critical update on the strategies towards bioactive compounds with emphasis on lapachones. Eur. J. Med. Chem. **179**, 863–915 (2019) https://doi.org/10.1016/j.ejmech.2019.06.056

[25] Porta, E.O.J., Kalesh, K., Steel, P.G.: Navigating drug repurposing for Chagas disease: advances, challenges, and opportunities. Front. Pharmacol. **14** (2023) https://doi.org/10.3389/fphar.2023.1233253

[26] Salomao, K., Figueiredo Sadok Menna-Barreto, R., Lisboa de Castro, S.: Stairway to Heaven or Hell? Perspectives and Limitations of Chagas Disease Chemotherapy. Curr. Top. Med. Chem. **16**(20), 2266–2289 (2016) https://doi.org/10.2174/1568026616666160413125049

[27] Khan, A.A., Langston, H.C., Walsh, L., Roscoe, R., Jayawardhana, S., Francisco, A.F., Taylor, M.C., McCann, C.J., Kelly, J.M., Lewis, M.D.: Enteric nervous system regeneration and functional cure of experimental digestive Chagas disease with trypanocidal chemotherapy. Nat. Commun. **15**(1), 4400 (2024) https://doi.org/10.1038/s41467-024-48749-5

[28] Junior, P.A.S., Molina, I., Murta, S.M.F., Sánchez-Montalvá, A., Salvador, F., Corrêa-Oliveira, R., Carneiro, C.M.: Experimental and clinical treatment of chagas disease: A review. The American Journal of Tropical Medicine and Hygiene **97**, 1289–1303 (2017) https://doi.org/10.4269/ajtmh.16-0761

[29] Bern, C.: Antitrypanosomal therapy for chronic chagas' disease. New England Journal of Medicine **364**, 2527–2534 (2011) https://doi.org/10.1056/NEJMct1014204

[30] Molina, I., Salvador, F., Sánchez-Montalvá, A., Treviño, B., Serre, N., A, S.A., Almirante, B.: Toxic profile of benznidazole in patients with chronic chagas disease: Risk factors and comparison of the product from two different manufacturers. Antimicrobial Agents and Chemotherapy **59**, 6125–6131 (2015) https://doi.org/10.1128/aac.04660-14

[31] Hasslocher-Moreno, A.M., Brasil, P.E.A.A., Sousa, A.S., Xavier, S.S., Chambela, M.C., Silva, G.M.S.: Safety of benznidazole use in the treatment of chronic chagas' disease. Journal of Antimicrobial Chemotherapy **67**, 1261–1266 (2012) https://doi.org/10.1093/jac/dks027

[32] Lindner, A.K., Lejon, V., Chappuis, F., Seixas, J., Kazumba, L., Barrett, M.P., Mwamba, E., Erphas, O., Akl, E.A., Villanueva, G., Bergman, H., Simarro, P., Kadima Ebeja, A., Priotto, G., Franco, J.R.: New WHO guidelines for treatment of gambiense human African trypanosomiasis including fexinidazole: substantial changes for clinical practice. Lancet Infect. Dis. **20**(2), 38–46 (2020) https://doi.org/10.1016/S1473-3099(19)30612-7

[33] Lindner, A.K., Lejon, V., Barrett, M.P., Blumberg, L., Bukachi, S.A., Chancey, R.J., Edielu, A., Matemba, L., Mesha, T., Mwanakasale, V., Pasi, C., Phiri, T., Seixas, J., Akl, E.A., Probyn, K., Villanueva, G., Simarro, P.P., Kadima Ebeja, A., Franco, J.R., Priotto, G.: New WHO guidelines for treating rhodesiense human African trypanosomiasis: expanded indications for fexinidazole and pentamidine. Lancet Infect. Dis. **25**(2), 77–85 (2025) https://doi.org/10.1016/S1473-3099(24)00581-4

[34] Oliveira, J.C., Abreu, B.U., Paz, E.R.S., Almeida, R.G., Honorato, J., Souza, C.P., Fantuzzi, F., Ramos, V.F.S., Menna-Barreto, R.F.S., Araujo, M.H., Jardim, G.A.M., Silva Júnior, E.N.: Sufex-functionalized quinones via ruthenium-catalyzed c−h alkenylation: A potential building block for bioactivity valorization. Chemistry – An Asian Journal **19**, 202400757 (2024) https://doi.org/10.1002/asia.202400757

[35] Paz, E.R.S., Souza, C.P., De Oliveira, J.C., Almeida, R.G., Herrera-Acevedo, C., Lakoh, S., Jardim, G.A.M., da Silva Júnior, E.N., Fantuzzi, F.: Ruthenium-Catalyzed C–H Alkenylation of Trypanocidal Naphthoquinones: A Mechanistic Benchmarking Study. ChemistryOpen **15**(2), 202500465 (2026) https://doi.org/10.1002/open.202500465

[36] Barrow, A.S., Smedley, C.J., Zheng, Q., Li, S., Dong, J., Moses, J.E.: The growing applications of sufex click chemistry. Chemical Society Reviews **48**, 4731–4758 (2019) https://doi.org/10.1039/C8CS00960K

[37] Sonani, R.R., Blat, A., Jemiola-Rzeminska, M., Lipinski, O., Patel, S.N., Sood, T., Dubin, G.: Structure of trypanosoma peroxisomal import complex unveils conformational heterogeneity. Nature Communications **16**, 11398 (2025) https://doi.org/10.1038/s41467-025-66207-8

[38] Eberhardt, J., Santos-Martins, D., Tillack, A.F., Forli, S.: Autodock vina 1.2.0: New docking methods, expanded force field, and python bindings. Journal of Chemical Information and Modeling **61**, 3891–3898 (2021) https://doi.org/10.1021/acs.jcim.1c00203

[39] Trott, O., Olson, A.J.: Autodock vina: Improving the speed and accuracy of docking with a new scoring function, efficient optimization, and multithreading. Journal of Computational Chemistry **31**, 455–461 (2010) https://doi.org/10.1002/jcc.21334

[40] Dennington, R., Keith, T.A., Millam, J.M.: GaussView Version 6. Semichem Inc. Shawnee Mission KS (2019)

[41] Chai, J.-D., Head-Gordon, M.: Long-range corrected hybrid density functionals with damped atom–atom dispersion corrections. Physical Chemistry Chemical Physics **10**(44), 6615–6620 (2008) https://doi.org/10.1039/B810189B

[42] Weigend, F., Ahlrichs, R.: Balanced basis sets of split valence, triple zeta valence and quadruple zeta valence quality for h to rn: Design and assessment of accuracy. Phys. Chem. Chem. Phys. **7**, 3297–3305 (2005) https://doi.org/10.1039/b508541a

[43] Frisch, M.J., Trucks, G.W., Schlegel, H.B., Scuseria, G.E., Robb, M.A., Cheeseman, J.R., Scalmani, G., Barone, V., Petersson, G.A., Nakatsuji, H., Li, X., Caricato, M., Marenich, A.V., Bloino, J., Janesko, B.G., Gomperts, R., Mennucci, B., Hratchian, H.P., Ortiz, J.V., Izmaylov, A.F., Sonnenberg, J.L., Williams-Young, D., Ding, F., Lipparini, F., Egidi, F., Goings, J., Peng, B., Petrone, A., Henderson, T., Ranasinghe, D., Zakrzewski, V.G., Gao, J., Rega, N., Zheng, G., Liang, W., Hada, M., Ehara, M., Toyota, K., Fukuda, R., Hasegawa, J., Ishida, M., Nakajima, T., Honda, Y., Kitao, O., Nakai, H., Vreven, T., Throssell, K., Montgomery, J.A. Jr., Peralta, J.E., Ogliaro, F., Bearpark, M.J., Heyd, J.J., Brothers, E.N., Kudin, K.N., Staroverov, V.N., Keith, T.A., Kobayashi, R., Normand, J., Raghavachari, K., Rendell, A.P., Burant, J.C., Iyengar, S.S., Tomasi, J., Cossi,

M., Millam, J.M., Klene, M., Adamo, C., Cammi, R., Ochterski, J.W., Martin, R.L., Morokuma, K., Farkas, O., Foresman, J.B., Fox, D.J.: Gaussian˜16 Revision C.01. Gaussian Inc. Wallingford CT (2016)

[44] Pettersen, E.F., Goddard, T.D., Huang, C.C., Couch, G.S., Greenblatt, D.M., Meng, E.C., Ferrin, T.E.: Ucsf chimera—a visualization system for exploratory research and analysis. Journal of Computational Chemistry **25**, 1605–1612 (2004) https://doi.org/10.1002/jcc.20084

[45] Grand, S.L., Götz, A.W., Walker, R.C.: Spfp: Speed without compromise—a mixed precision model for gpu accelerated molecular dynamics simulations. Computer Physics Communications **184**, 374–380 (2013) https://doi.org/10.1016/j.cpc.2012.09.022

[46] Götz, A.W., Williamson, M.J., Xu, D., Poole, D., Grand, S.L., Walker, R.C.: Routine microsecond molecular dynamics simulations with amber on gpus. 1. generalized born. Journal of Chemical Theory and Computation **8**, 1542–1555 (2012) https://doi.org/10.1021/ct200909j

[47] Case, D.A., Aktulga, H.M., Belfon, K., Cerutti, D.S., Cisneros, G.A., Cruzeiro, V.W.D., Forouzesh, N., Giese, T.J., Götz, A.W., Gohlke, H., Izadi, S., Kasavajhala, K., Kaymak, M.C., King, E., Kurtzman, T., Lee, T.-S., Li, P., Liu, J., Luchko, T., Luo, R., Manathunga, M., Machado, M.R., Nguyen, H.M., O'Hearn, K.A., Onufriev, A.V., Pan, F., Pantano, S., Qi, R., Rahnamoun, A., Risheh, A., Schott-Verdugo, S., Shajan, A., Swails, J., Wang, J., Wei, H., Wu, X., Wu, Y., Zhang, S., Zhao, S., Zhu, Q., Cheatham, T.E.I.I.I., Roe, D.R., Roitberg, A., Simmerling, C., York, D.M., Nagan, M.C., Merz, K.M.J.: Ambertools. Journal of Chemical Information and Modeling **63**, 6183–6191 (2023) https://doi.org/10.1021/acs.jcim.3c01153

[48] Maier, J.A., Martinez, C., Kasavajhala, K., Wickstrom, L., Hauser, K.E., Simmerling, C.: ff14sb: Improving the accuracy of protein side chain and backbone parameters from ff99sb. Journal of Chemical Theory and Computation **11**, 3696–3713 (2015) https://doi.org/10.1021/acs.jctc.5b00255

[49] Jorgensen, W.L., Chandrasekhar, J., Madura, J.D., Impey, R.W., Klein, M.L.: Comparison of simple potential functions for simulating liquid water. The Journal of Chemical Physics **79**, 926–935 (1983) https://doi.org/10.1063/1.445869

[50] Salomon-Ferrer, R., Götz, A.W., Poole, D., Grand, S.L., Walker, R.C.: Routine microsecond molecular dynamics simulations with amber on gpus. 2. explicit solvent particle mesh ewald. Journal of Chemical Theory and Computation **9**, 3878–3888 (2013) https://doi.org/10.1021/ct400314y

[51] Ryckaert, J.-P., Ciccotti, G., Berendsen, H.J.C.: Numerical integration of the cartesian equations of motion of a system with constraints: molecular dynamics of n-alkanes. Journal of Computational Physics **23**, 327–341 (1977) https://doi.org/10.1016/0021-9991(77)90098-5

[52] Pastor, R.W., Brooks, B.R., Szabo, A.: An analysis of the accuracy of langevin and molecular dynamics algorithms. Molecular Physics **65**, 1409–1419 (1988) https://doi.org/10.1080/00268978800101881

[53] Roe, D.R., Cheatham, T.E.I.I.I.: Ptraj and cpptraj: Software for processing and analysis of molecular dynamics trajectory data. Journal of Chemical Theory and Computation **9**, 3084–3095 (2013) https://doi.org/10.1021/ct400341p

[54] Wang, J., Wang, W., Kollman, P.A., Case, D.A.: Automatic atom type and bond type perception in molecular mechanical calculations. Journal of Molecular Graphics and Modelling **25**(2), 247–260 (2006) https://doi.org/10.1016/j.jmgm.2005.12.005

[55] Bayly, C.I., Cieplak, P., Cornell, W., Kollman, P.A.: A well-behaved electrostatic potential based method using charge restraints for deriving atomic charges: the resp model. The Journal of Physical Chemistry **97**, 10269–10280 (1993) https://doi.org/10.1021/j100142a004

[56] Kollman, P.A., Massova, I., Reyes, C., Kuhn, B., Huo, S., Chong, L., Lee, M., Lee, T., Duan, Y., Wang, W., Donini, O., Cieplak, P., Srinivasan, J., Case, D.A., Cheatham, T.E.: Calculating structures and free energies of complex molecules:combining molecular mechanics and continuum models. Accounts of Chemical Research **33**, 889–897 (2000) https://doi.org/10.1021/ar000033j

[57] Hansson, T., Marelius, J., Åqvist, J.: Ligand binding affinity prediction by linear interaction energy methods. Journal of Computer-Aided Molecular Design **12**, 27–35 (1998) https://doi.org/10.1023/A:1007930623000

[58] Miller, B.R.I.I.I., McGee, T.D.J., Swails, J.M., Homeyer, N., Gohlke, H., Roitberg, A.E.: Mmpbsa.py: An efficient program for end-state free energy calculations. Journal of Chemical Theory and Computation **8**, 3314–3321 (2012) https://doi.org/10.1021/ct300418h

[59] Kumar Jha, R., Kumar, S.: Direct Functionalization of para -Quinones: A Historical Review and New Perspectives. European J. Org. Chem. **27**(27), 202400535 (2024) https://doi.org/10.1002/ejoc.202400535

[60] Müller, L., Poll, J., Nuernberger, P., Ghosh, I., König, B.: Quinones as Multifunctional Scaffolds for Oxidative, Reductive, and HAT Photocatalysis. Chem. – A Eur. J. **31**(20), 202404707 (2025) https://doi.org/10.1002/chem.202404707

[61] Krieger, I.V., Sukheja, P., Yang, B., Tang, S., Selle, D., Woods, A., Engelhart, C., Kumar, P., Harbut, M.B., Liu, D., Tsuda, B., Qin, B., Bare, G.A.L., Li, G., Chi, V., Gambacurta, J., Hvizdos, J., Reagan, M., Jones, I.L., Massoudi, L.M., Woolhiser, L.K., Cascioferro, A., Kundrick, E., Singh, P., Reiley, W., Ioerger, T.R., Kandula, D.R., McCabe, J.W., Guo, T., Alland, D., Boshoff, H.I., Schnappinger, D., Robertson, G.T., Mdluli, K., Lee, K.-J., Dong, J., Li, S., Schultz, P.G., Joseph, S.B., Love, M.S., Sharpless, K.B., Petrassi, H.M., Chatterjee, A.K., Sacchettini, J.C., McNamara, C.W.: SuFEx-based antitubercular compound irreversibly inhibits Pks13. Nature **645**(8081), 755–763 (2025) https://doi.org/10.1038/s41586-025-09286-3

[62] Bolton, J.L., Trush, M.A., Penning, T.M., Dryhurst, G., Monks, T.J.: Role of Quinones in Toxicology. Chem. Res. Toxicol. **13**(3), 135–160 (2000) https://doi.org/10.1021/tx9902082

[63] El-Najjar, N., Gali-Muhtasib, H., Ketola, R.A., Vuorela, P., Urtti, A., Vuorela, H.: The chemical and biological activities of quinones: overview and implications in analytical detection. Phytochem. Rev. **10**(3), 353–370 (2011) https://doi.org/10.1007/s11101-011-9209-1

[64] Cores, Á., Carmona-Zafra, N., Clerigué, J., Villacampa, M., Menéndez, J.C.: Quinones as Neuroprotective Agents. Antioxidants **12**(7), 1464 (2023) https://doi.org/10.3390/antiox12071464

[65] Lu, J.-J., Bao, J.-L., Wu, G.-S., Xu, W.-S., Huang, M.-Q., Chen, X.-P., Wang, Y.-T.: Quinones derived from plant secondary metabolites as anti-cancer agents. Anti-Cancer Agents Med. Chem. **13**(3), 456–463 (2013)

[66] Kayser, O., Kiderlen, A.F., Croft, S.L.: Natural products as antiparasitic drugs. Parasitol. Res. **90**, 55–62 (2003) https://doi.org/10.1007/s00436-002-0768-3

[67] Md Mumtaz, S., Shahrukh, M., Bhardwaj, G., Altamish, M.: Quinones as potential therapeutic agents for metabolic disorders. In: Dar, U.A., Shahnawaz, M., Hakeem, K.R. (eds.) Quinone-Based Compounds in Drug Discovery: Trends and Applications, pp. 169–190. Elsevier, Amsterdam, Netherlands (2025). https://doi.org/10.1016/B978-0-443-24126-0.00010-X

[68] Ioset, J.-R.: Natural Products for Neglected Diseases: A Review. Curr. Org. Chem. **12**(8), 643–666 (2008) https://doi.org/10.2174/138527208784577394

[69] Wood, J.M., Carvalho, R.L., da Silva Júnior, E.N.: The Different Facets of Metal-Catalyzed C–H Functionalization Involving Quinone Compounds. Chem. Rec. **21**(10), 2604–2637 (2021) https://doi.org/10.1002/tcr.202000163

[70] Ventura Pinto, A., Lisboa de Castro, S.: The Trypanocidal Activity of Naphthoquinones: A Review. Molecules **14**(11), 4570–4590 (2009) https://doi.org/10.3390/molecules14114570

[71] Menna-Barreto, R.F.S., Goncalves, R.L.S., Costa, E.M., Silva, R.S.F., Pinto, A.V., Oliveira, M.F., Castro, S.L.: The effects on Trypanosoma cruzi of novel synthetic naphthoquinones are mediated by mitochondrial dysfunction. Free Radic. Biol. Med. **47**(5), 644–653 (2009) https://doi.org/10.1016/j.freeradbiomed.2009.06.004

[72] Silva Júnior, E.N., Jardim, G.A.M., Menna-Barreto, R.F.S., Castro, S.L.: Anti- Trypanosoma cruzi Compounds: Our Contribution for the Evaluation and Insights on the Mode of Action of Naphthoquinones and Derivatives. J. Braz. Chem. Soc. (2014) https://doi.org/10.5935/0103-5053.20140180

[73] Bombaça, A.C.S., Viana, P.G., Santos, A.C.C., Silva, T.L., Rodrigues, A.B.M., Guimarães, A.C.R., Goulart, M.O.F., da Silva Júnior, E.N., Menna-Barreto, R.F.S.: Mitochondrial disfunction and ROS production are essential for anti-Trypanosoma cruzi activity of β-lapachone-derived naphthoimidazoles. Free Radic. Biol. Med. **130**, 408–418 (2019) https://doi.org/10.1016/j.freeradbiomed.2018.11.012

[74] Jin, X., Lee, K., Kim, N.H., Kim, H.S., Yook, J.I., Choi, J., No, K.T.: Natural products used as a chemical library for protein–protein interaction targeted drug discovery. J. Mol. Graph. Model. **79**, 46–58 (2018) https://doi.org/10.1016/j.jmgm.2017.10.015

[75] Meng, N., Tang, H., Zhang, H., Jiang, C., Su, L., Min, X., Zhang, W., Zhang, H., Miao, Z., Zhang, W., Zhuang, C.: Fragment-growing guided design of Keap1-Nrf2 protein-protein interaction inhibitors for targeting myocarditis. Free Radic. Biol. Med. **117**, 228–237 (2018) https://doi.org/10.1016/j.freeradbiomed.2018.02.010

[76] Lauriola, A., Uliassi, E., Santucci, M., Bolognesi, M.L., Mor, M., Scalvini, L., Elisi, G.M., Gozzi, G., Tagliazucchi, L., Marverti, G., Ferrari, S., Losi, L., D'Arca, D., Costi, M.P.: Identification of a Quinone Derivative as a YAP/TEAD Activity Modulator from a Repurposing Library. Pharmaceutics **14**(2), 391 (2022) https://doi.org/10.3390/pharmaceutics14020391

[77] Jayatunga, M.K.P., Thompson, S., McKee, T.C., Chan, M.C., Reece, K.M., Hardy, A.P., Sekirnik, R., Seden, P.T., Cook, K.M., McMahon, J.B., Figg, W.D., Schofield, C.J., Hamilton, A.D.: Inhibition of the HIF1α-p300 interaction by quinone- and indandione-mediated ejection of structural Zn(II). Eur. J. Med. Chem. **94**, 509–516 (2015) https://doi.org/10.1016/j.ejmech.2014.06.006

[78] Machado, T.M., Souza, D.E.M., Soares, J.T.T., Guilhon-Simplicio, F.: Ai-driven in silico screening of lapachol derivatives as potential therapeutics against chagas disease. In: III Simpósio do CI-IA Saúde da UFMG: Inteligência Artificial Responsável na Saúde. Da Pesquisa à Prática Clínica, Belo Horizonte, MG, Brazil, pp. 10–12 (2025)

Supplementary Files

This is a list of supplementary files associated with this preprint. Click to download.

- SupplementarymaterialAMD.pdf